Are dense networks of low-cost nodes really useful for monitoring air pollution? A case study in Staffordshire

Louise Bøge Frederickson[1, 2, 3], Ruta Sidaraviciute[3], Johan Albrecht Schmidt[3], Ole Hertel[5], and Matthew Stanley Johnson[3, 4]

[1]Department of Environmental Science, Aarhus University, Frederiksborgvej 399, DK-4000 Roskilde, Denmark
[2]Danish Big Data Centre for Environment and Health (BERTHA), Aarhus University, Frederiksborgvej 399, DK-4000 Roskilde, Denmark
[3]AirLabs Denmark, Nannasgade 28, DK-2200 Copenhagen N, Denmark
[4]Department of Chemistry, University of Copenhagen, Universitetsparken 5, DK-2100 Copenhagen Ø, Denmark
[5]Department of Ecoscience, Aarhus University, Frederiksborgvej 399, DK-4000 Roskilde, Denmark

Correspondence: Matthew Stanley Johnson (msj@chem.ku.dk)

Abstract. Air pollution exhibits hyper-local variation, especially near emissions sources. In addition to people's time-activity patterns, this variation is the most critical element determining exposure. Pollution exposure is time-activity and path-dependent with specific behaviors such as mode of commuting and time spent near a roadway or in a park playing a decisive role. Compared to conventional air pollution monitoring stations, nodes containing low-cost air pollution sensors can be deployed with very high density. In this study, a network of 18 nodes using low-cost air pollution sensors was deployed in Newcastle-under-Lyme, Staffordshire, UK, in June 2020. Each node measured a range of species including nitrogen dioxide (NO_2), ozone (O_3) and particulate matter ($PM_{2.5}$ and PM_{10}); this study focuses on NO_2 and $PM_{2.5}$ over a one year period from August 1, 2020 to October 1, 2021. A simple and effective temperature, scale and offset correction was able to overcome data quality issues associated with temperature bias in the NO_2 readings. In its recent update, the World Health Organization dramatically reduced annual exposure limit values from 40 to 10 $\mu g\ m^{-3}$ for NO_2 and from 10 to 5 $\mu g\ m^{-3}$ for $PM_{2.5}$. We found the average annual mean NO_2 concentration for the network was 17.5 $\mu g\ m^{-3}$, and 8.1 $\mu g\ m^{-3}$ for $PM_{2.5}$. While in exceedance of the WHO guideline levels, these average concentrations do not exceed legally binding UK/EU standards. The network average NO_2 concentration was 12.5 $\mu g\ m^{-3}$ higher than values reported by a nearby regional air quality monitoring station, showing the critical importance of monitoring close to sources before pollution is diluted. We demonstrate how data from a low-cost air pollution sensor network can reveal insights into patterns of air pollution and help determine whether sources are local or non-local. With spectral analysis, we investigate the variation of the pollution levels and identify typical periodicities. Both NO_2 and $PM_{2.5}$ have contributions from high-frequency sources, however, the low-frequency sources are significantly different. Using spectral analysis, we determine that at least 54.3 $\pm$ 4.3 % of NO_2 is from local sources, whereas in contrast, only 37.9 $\pm$ 3.5 % of $PM_{2.5}$ is local.

1 Introduction

According to the World Health Organization (WHO), seven million premature deaths every year can be attributed to poor air quality (Lelieveld, 2015; WHO, 2021). In response to the adverse health effects caused by air pollution, the WHO developed Air Quality Guidelines (AQGs) for a set of key air pollutants, including nitrogen dioxide (NO_2) and particulate matter with an aerodynamic diameter ≤ 2.5 μm ($PM_{2.5}$) (WHO, 2021). Since WHO's 2015 recommendation, evidence has accumulated showing many additional negative impacts of air pollution on health (Abdo, 2016; Sun, 2016; Chen, 2018; Ai, 2019; Wang, 2019; Wu, 2019; Zhang, 2020). After a comprehensive review of the evidence the WHO has recently recommended a much more strict set of standards and warned that exceeding the new air quality guideline levels is associated with significant health risks. **Table 1** shows the previous and revised AQGs for the pollutants of focus within this study along with the EU standards. These standards are legally binding, while the WHO values are indicative.

Traditionally, air quality monitoring is based on static air quality monitoring stations (AQMS) with calibrated high-precision instruments. However, due to their purchase and maintenance costs, conventional AQMSs are generally sparsely located (Kumar, 2015; Maag, 2018). This monitoring strategy is suited to characterizing regional air quality but could fail to account for elevated concentrations near sources. Moreover the temporal and spatial resolution of such monitoring station networks is limited (Motlagh, 2020). For example there are a total of 18 AQMSs in the nation of Denmark, responsible for measuring concentrations at street level, urban background and regions (Danish National Monitoring Program for Water and Nature (NOVANA) (Ellermann, 2018)).

Meanwhile, field studies have shown that pollution levels, especially in urban environments, can vary substantially within a few meters due to localized air pollution sources (Lebret, 2000; Kingham, 2000; Monn, 2001; Zou, 2009; Wang, 2018; Li, 2019; Wilson, 2019). The local component can often be an important factor contributing to people's exposure, for example, for those who commute in a vehicle and/or work as professional drivers, street police, bicycle delivery etc. (Frederickson, 2020a), or live or work in buildings near busy roads. Low-cost air pollution sensors and sensor networks have evolved rapidly during the last few decades, enabled by technological progress and the development of fast and inexpensive wireless communication systems (Snyder, 2013). While the technologies are still evolving, low-cost air pollution sensors are becoming available and are starting to become a valuable supplement to the sparse conventional AQMS. Low-cost sensor (LCS) based networks are

Pollutant	EU		AQGs 2015		AQGs 2021	
	Averaging period	Concentration	Averaging period	Concentration	Averaging period	Concentration
NO_2	Annual mean	40	Annual mean	40	Annual mean	10
	1-hour mean	200	1-hour mean	200	24-hour mean	25
$PM_{2.5}$	Annual mean	25	Annual mean	10	Annual mean	5
			24-hour mean	25	24-hour mean	15

Table 1. Air quality standards set by the European Union (Gemmer, 2013) and WHO's global air quality guidelines (AQGs) from 2015 and 2021 (WHO, 2021). All concentrations are in μg m^{-3}.

not a substitute for networks of conventional AQMSs, since high-quality monitoring data is necessary for checking compliance with guidelines and they are also necessary for validating less expensive mapping obtained from modelling and/or LCS based monitoring.

Networks of low-cost air pollution sensors are becoming more common. On a device level, clearly the sensor elements cannot compete with commercial instruments regarding The Three 'S's: Sensitivity, Stability, and Selectivity (Lewis, 2016; Borrego, 2016; Castell, 2017; Frederickson, 2020b), this may be more than compensated because LCSs enable greatly increased site density and temporal resolution, facilitating new insights into patterns and sources of air pollution. In addition, LCSs can supplement not only coarse-scale monitoring networks but also add substantial value to mappings provided by mathematical models. Dense networks of LCSs can be used for source apportionment and to distinguish local from non-local pollution (Heimann, 2015), and as an aid in interpreting mathematical models that are often an integrated part of air quality monitoring (Hertel, 2007).

Within this study, electrochemical LCSs are used to measure gaseous pollutants and laser based particle counters are used to quantify particulate matter. Electrochemical sensor technology offers a number of advantages including linear response, small size, low cost in fabrication, relatively fast response, and low power consumption (Frederickson, 2020b). While low-cost air pollution sensors bring new opportunities for monitoring, important issues remain regarding data quality. Studies show that sensor data can be influenced by environmental factors such as temperature and confounding gases (Spinelle, 2015, 2017; Mead, 2013; Bulot, 2020). Considerable efforts have been made to understand these factors, with varying success. Field work presents a complex and dynamic environment, greatly complicating the task of calibration. Experience shows that it is crucial to test each individual sensor and correct for multiple ambient factors (Popoola, 2016).

While a time series analysis based on summary statistics is a simple and effective tool, more sophisticated techniques are necessary to better understand the ultimate causes of these variations (Hwang, 2000). Spectral analysis using the Fourier transform can provide a deeper understanding of time series, because transformation into the frequency domain allows characterization of sources according to their periodicity and rate of change (Percival, 1998). While spectral analysis has long been used for meteorological variables, because of its ability to distinguish synoptic and seasonal signals (Van der Hoven, 1957; Lyons, 1975; Eskridge, 1997), studies applying the Fourier transform to air pollution data emerged much later (Rao, 1976; Hogrefe, 2006; Choi, 2008; Lazi, 2016).

There is a relation between temporal and spatial scales of air pollution (Brasseur, 2017). Analysis of air quality data in the frequency domain contributes to the understanding of periodic behaviors and yields information about spatial and temporal scales of the hidden, underlying mechanisms (Hies, 2000; Sebald, 2000; Marr, 2002). Short-term fluctuations of the pollutant concentrations are related to local-scale phenomena, including local dispersion conditions and patterns in local emissions and chemistry. Conversely, seasonal changes and the long-range transport and emissions of pollutants contribute to the spectrum at very low frequencies (Tchepel, 2009). On the time-scale of days, there are the motions of weather systems for example a high pressure system with well-developed photochemical air pollution. Pollution arriving from a distant source is characterized by a slowly rising and falling signal due to the effects of transport time and atmospheric mixing. Regional emissions are of course regional in scale and photochemical pollution typically develops in a synoptic air mass. In contrast local sources (e.g. traffic)
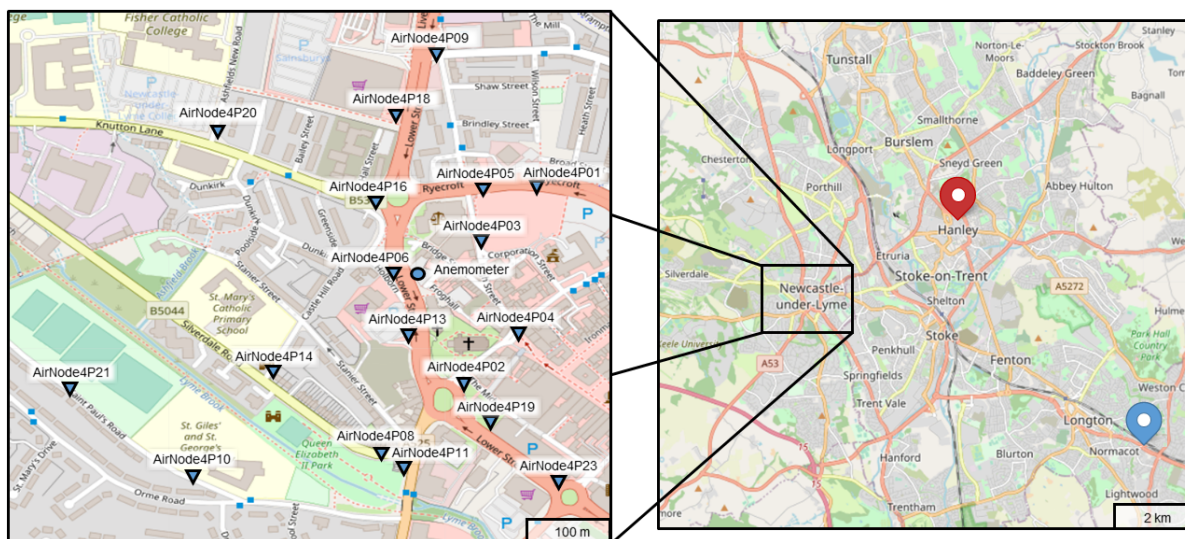
Figure 1. Spatial distribution of the AirNode network (left) and an overview of the location of the network relative to the two closest reference stations (right). The urban background station at Stoke-on-Trent Center is highlighted with a red marker, whereas roadside monitoring station at Stoke-on-Trent A50 Roadside is highlighted with a blue marker. The last AQMS used in this study (regional background monitoring station at Ladybower) is located 54 km from the network and is for clarity not included on the map. Maps obtained from ©OpenStreetMap contributors 2021. Distributed under the Open Data Commons Open Database License (ODbL) v1.0 (OpenStreetMap, 2021).

80 more often present as a sharp spike in concentration. Even an instantaneous puff of pollution will broaden with time based on the vertical and horizontal eddy diffusion coefficients, K, which are on the order of 100 m^2 s^{-1} (Seinfeld and Pandis, 2016).

In this paper, we show how low-cost air pollution sensors provide additional insights into the patterns and sources of air pollution when deployed as a network rather than as individual sensors. A low-cost air pollution sensor network consisting of 18 low-cost air pollution sensor nodes (called *AirNode4PX*) was deployed in Newcastle-under-Lyme, UK, in the area centered

85 around the ring road (see **Figure 1**). The variation in road width, the different types of road structure, and highly variable traffic patterns all impact pollutant dispersion, resulting in significant spatiotemporal variation of pollution in the area. Each AirNode measured a range of species including nitrogen dioxide (NO_2), ozone (O_3) and particulate matter ($PM_{2.5}$ and PM_{10}); in this paper we focus on NO_2 and $PM_{2.5}$. This paper does not attempt to demonstrate that the low-cost air pollution sensors meet specific air quality monitoring standards. Rather, we argue that data obtained from such a network is able to provide useful

90 additional information about local air pollution that extends what can be learned from conventional air quality monitoring stations. The data obtained from the low-cost air pollution sensor network is used for time series analysis in the frequency domain to obtain information on the variability of air pollution concentrations and to distinguish local sources from regional. The network, together with the analysis approach, has allowed pollutant emissions attributable solely to the local sources to be distinguished from other regional or long-range transport sources. The approach of frequency domain analysis will be further

95 evaluated in subsequent studies.

2 Field trial of the Staffordshire network

In June 2020, a network of 18 air pollution sensor nodes containing low-cost electrochemical and metal oxide gas sensors and optical particle counters was deployed in Newcastle-under-Lyme in Staffordshire, UK, in the area centered around the ring road. In addition, an anemometer was installed to record wind speed and direction. The initial 14 day installation, stabilization and testing period of the measurement campaign are excluded from the analysis. In all the study covers a 14-month period from August 1, 2020 to October 1, 2021.

2.1 Nodes of low-cost air pollution sensors

The nodes include low-cost air pollution sensors, signal processing and communications. The units, $88 \times 88 \times 90$ mm, are assembled by AirLabs into weatherproof enclosures with full exposure to ambient air, and are set up to report measurements to a cloud hosted by Amazon Web Services. The low-cost air pollution sensor nodes are generation 4P and are referred to as *AirNode*, *AirNode4PX* or *4PX*, with X being the node number. Each AirNode includes sensors for measuring NO_2 (NO2-B43F from Alphasense Ltd.) and O_3 (MiCS-6814 from SGX Sensortech) as well as $PM_{2.5}$ and PM_{10} (SDS-011 from Nova Fitness Co.) at a 1-min time-resolution. In addition, each node is equipped with a control board and micro-controller unit (ESP32) for programming the sensors. The AirNodes were laboratory tested in Copenhagen, Denmark, to validate their response and obtain laboratory-based calibration coefficients, which are used to interpret the preliminary data. After laboratory calibration the AirNodes were shipped to Newcastle-under-Lyme in Staffordshire, United Kingdom, and were mounted 2.5 to 3 m above street level on lamp posts which also provided power as shown in **Figure 1**. Since the study focuses on NO_2 and $PM_{2.5}$, a brief description of the sensors is given below.

The SDS-011 sensor (Nova Fitness Co. Ltd, 2015) is a low-cost air pollution sensor measuring $PM_{2.5}$ and PM_{10}. Its principle of operation is based on light scattering (van de Hulst, 1981), where particle density distribution is determined using the intensity distribution patterns produced when particles scatter a laser beam (Liu, 2019). The sensor module includes a fan to ensure a continuous flow of air through the sensor chamber (Genikomsakis, 2018). An algorithm converts the particle density distribution into particle mass, and it can measure the particle density distribution between 0.3 to 10 μm (Bulot, 2020; Budde, 2018).

For NO_2 measurements, the NO2-B43F sensor (Alphasense, 2019) is used. This is an amperometric electrochemical gas sensor containing four electrodes, where the principle of operation is based on electrochemistry (Frederickson, 2020b). When the Working Electrode (WE) is exposed to ambient air, the target gas can diffuse onto the surface of the electrode, where it is chemically reduced, resulting in a change in current. The Counter Electrode balances the current, and the Reference Electrode sets the operating potential of WE. The fourth electrode is an Auxiliary Electrode (AE) and has the same structure as WE but is not exposed to ambient air, hence is not affected by the target gas concentration, only by environmental parameters such as temperature. Therefore, the difference in voltage between the WE and AE corresponds to changes in target gas concentration at the electrochemical cell surface. A trans-impedance amplifier converts the currents from the electrochemical cell into a voltage. The voltage is amplified further by a non-inverting operational amplifier, then a 16-bit analogue to digital (A/D) converter

(ADS1115) samples the output and produces a digital reading of the voltage level. This is used by the microprocessor to calculate the actual gas concentration (Cross, 2017; Stetter, 2008; Mead, 2013). To minimize possible cross-interference from ozone, the NO_2 sensors were fitted with integrated catalytic ozone filters (MnO_2 filters). The performance of these filters was verified in the laboratory, and the NO_2 sensors showed no significant response to ozone in the range of $0 - 100$ ppb. Cross-interferences from other common gas pollutants were not considered important based on prior studies (Sun, 2017; Mead, 2013).

2.2 Correction methodology

The calibration of the electrochemical sensors measuring NO_2 is known to vary at high ($>20°C$) and low ($< 0°C$) temperatures and with rapid temperature change (Alphasense, 2019; Popoola, 2016; Li, 2021). Therefore we apply a correction with coefficients determined by using a linear regression model:

$$NO_2 (cor_T) = a_0 + a_1 \cdot T + a_2 \cdot dT/dt + a_3 \cdot NO_2 (dv) \tag{1}$$

where NO_2 (dv) are the raw output obtained by the Alphasense NO_2 cell. The NO_2 (dv) readings are found from the voltage change in cell 2, which is determined by the difference between the WE and AE outputs, $WE2_v$ and $AE2_v$:

$$NO_2 (dv) = WE2_v - AE2_v \tag{2}$$

T is filtered temperature data obtained from the nearest reference station. Filtered temperature represents the temperature reading when ambient temperature exceeds $10°C$ and is transformed according to

$$f(t) = \begin{cases} 0 & \text{if } T < 10 \\ T - 10 & \text{otherwise} \end{cases} \tag{3}$$

and dT/dt is the rate of change of the filtered temperature. The temperature threshold of $10°C$ was chosen because the internal temperatures of the LCS nodes often exceed the ambient temperatures and the performance of the correction was sufficient. The linear regression coefficients, a_0, a_1, a_2 and a_3, are calculated using the method of multiple least squares, separately for each AirNode (Spinelle, 2017). In this formula a_3 is a measure of the sensor's sensitivity and a_0 is the offset of the sensor, whereas a_1 and a_2 are temperature correction coefficients.

All electrochemical sensors have a different inherent sensitivity, hence the NO_2 readings need to be scale-corrected. The scale-correction is carried out by multiplying the temperature-corrected NO_2 readings (NO_2 (cor_T)), from each AirNode, with α, which is the ratio between the 0.80 and 0.20 quantiles of the NO_2 readings obtained from the AirNodes ($Q_{\text{diff, AirNode}}$) and from the reference ($Q_{\text{diff, Reference}}$). The reference is the NO_2 readings obtained by chemiluminescence from the reference-grade instrument at the AQMS at Stoke-on-Trent Centre, 4.1 km from the network, from the same period as the measurements took place. All data from the reference station are used for the correction. The difference between the 0.80 and 0.20 quantiles is a

proxy for the variation obtained in the measurements.

$$Q_{\text{diff, AirNode}} = Q_{0.80,\text{ AirNode}} - Q_{0.20,\text{ AirNode}} \tag{4}$$

$$Q_{\text{diff, Reference}} = Q_{0.80,\text{ Reference}} - Q_{0.20,\text{ Reference}} \tag{5}$$

$$\alpha = Q_{\text{diff, Reference}} / Q_{\text{diff, AirNode}} \tag{6}$$

$$\text{NO}_2\,(\text{cor}_{T,S}) = \text{NO}_2\,(\text{cor}_T) \cdot \alpha \tag{7}$$

The offsets of the readings are determined by calculating the difference between the 0.25 quantile ($Q_{0.25}$) obtained from each AirNode ($Q_{0.25,\text{ AirNode}}$) and from the reference ($Q_{0.25,\text{ Reference}}$). Hence, the offset of the temperature- and scale-corrected reading ($\text{NO}_2\,(\text{cor}_{T,S})$) is adjusted by subtracting the calculated offset (β). The reference used in the offset-correction is the same as the one used for the scale-correction. The 0.25 quantile is a proxy for measured background concentration.

$$\beta = Q_{0.25,\text{ AirNode}} - Q_{0.25,\text{ Reference}} \tag{8}$$

$$\text{NO}_2\,(\text{cor}) = \text{NO}_2\,(\text{cor}_{T,S}) - \beta \tag{9}$$

where $\text{NO}_2\,(\text{cor}_{T,S})$ is the temperature- and scale-corrected NO_2 reading, and $\text{NO}_2\,(\text{cor})$ is the temperature-, offset- and scale-corrected NO_2 reading.

Regarding the SDS-011 $\text{PM}_{2.5}$ readings, outliers were removed by removing all values exceeding 5 times the standard deviation. Scale and offset correction was performed for $\text{PM}_{2.5}$ similar to the one for the NO_2 readings. However, there was no significant difference between the corrected and uncorrected $\text{PM}_{2.5}$ readings since the $\text{PM}_{2.5}$ readings were already highly correlated (mean $R^2 = 0.72$) with the reference readings from the Stoke-on-Trent Centre.

2.3 Comparison with regulatory air quality monitoring stations

The data obtained from the network is compared with data from the three nearest regulatory air quality monitoring stations: The roadside monitoring station at Stoke-on-Trent A50 Roadside (52.980436°N, 2.111898°W, 8.7 km from the network), the urban background monitoring station at Stoke-on-Trent Centre (53.028210°N, 2.175133°W, 4.1 km from the network) and the regional background monitoring station at Ladybower (53.403370°N, 1.752006°W, 54 km from the network). We do not expect perfect agreement but nonetheless the exercise is useful.

Ladybower is located in the Peak District National Park around 800 meters to the southwest of Ladybower reservoir. The nearest road is 20 meters from the station and is only used by the nearby farmsteads. The surrounding area is mainly open moorland. The urban background monitoring station located in Stoke-on-Trent is in the northern part of downtown Hanley. This station is located five meters from a road connected to a busy multi-story car parking facility (50 meters from the monitoring station). The surrounding area is open grass with a few trees and commercial properties. The A50 Potteries Way is a busy ring road which lies approximately 130 meters to the north-east of the monitoring site. The roadside monitoring station is located between the main road and a parallel side road, near a pedestrian footbridge, beside the dual carriageway A50 through Stoke. All three AQMSs are equipped with instruments for measuring NO_2 by chemiluminescence, but only Stoke-on-Trent Centre

measures PM$_{2.5}$. Hourly air pollution data from each monitoring station were manually downloaded using the UK-Air data selector (DEFRA, 2022).

2.4 Spectral analysis

Spectral analysis is widely used for investigating cycles and variations of pollutants in time series to reveal the sources of pollution (Marr, 2002; Lazi, 2016). Within spectral analysis, the Fourier transform is a powerful tool for analyzing time series including periodicities and rate of change. To use the method it is necessary to overcome obstacles including the often unevenly spaced time points in time series due to technical and practical problems during monitoring (Sun, 1996, 1997). The unequally spaced or missing data can be circumvented by applying the fast Fourier transform after filling the gaps and missing values with the mean. In addition, the linear trend in the time series is removed by subtracting the average concentration obtained by each LCS. The periodogram for a finite time series is calculated as the square of the magnitude of X

$$\Phi(\nu_k) = |X(k)|^2 = \left| \frac{1}{\sqrt{N}} \sum_{t=0}^{N-1} x_t e^{(-2\pi i \nu_k t)} \right|^2 \tag{10}$$

where $k = 0, 1, ..., N-1$, and N is the number of observations, x_t is the time series, and $\nu_k = k/N$. The periodogram indicates the strength of the signal as a function of frequency, while its spectrum over the frequency range corresponds to the variance of the time series data. Parseval's Theorem (Parseval, 1806; Narayanan, 2003) states that the energy, or in this case intensity, is conserved during Fourier transformation. Thus, the contribution of the different pollution sources can be quantified by integrating the peaks in the periodograms (Marr, 2002).

There is a relationship between temporal and spatial scales of the different air pollutants. Rapid, short-term fluctuations of the pollutant concentrations happen as a result of local phenomena, e.g. local-scale dispersion, local emissions and short-term atmospheric chemistry. Rapid changes contribute to the periodogram at high frequencies, which, in this work are defined as
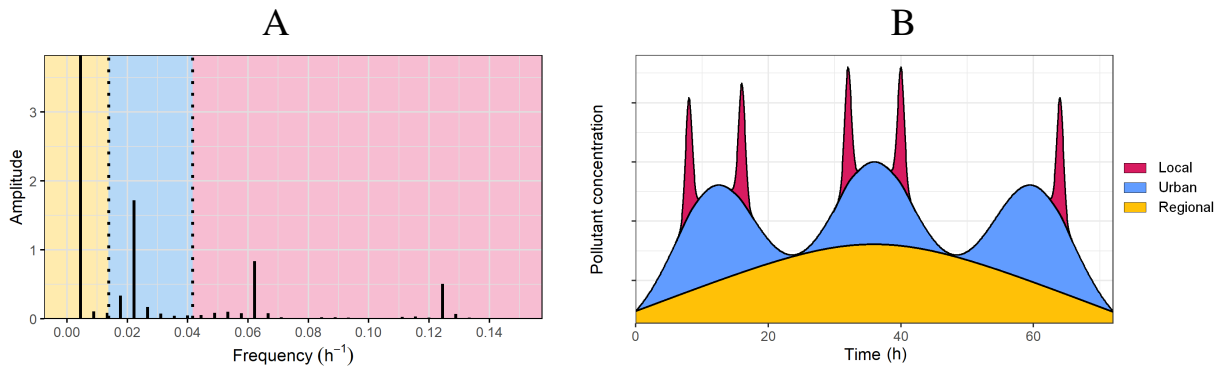
Figure 2. A. A periodogram showing short-term fluctuations at the high frequencies (red), background signals at low frequencies (yellow) and the fluctuations in-between (blue). **B.** Schematic illustration of air pollutant contribution from regional transport (yellow), the urban area (blue), and the street (red). The relative concentration of the contributions depends on the considered pollutant and the dispersion conditions.

above 0.0417 h^{-1}, i.e., events with a frequency higher/shorter than one day. This is referred to as the 'local' contribution to the pollutant concentration. The local-cutoff is chosen based on the European Environment Agency's definition of local time scale (EEA, 2008). The seasonal changes in the emissions and long-range transport of the pollution contribute to the periodogram at low frequencies (< 0.0139 h^{-1}), i.e., events with a frequency lower/longer than three days. This is then referred to as the 'regional' contribution to the pollutant concentration. In this model, intermediate frequencies are due to the 'urban' contribution to the pollutant concentration. The cutoff frequency for the regional contribution is based on the intercontinental transport, which occurs on timescales on the order of three days to one month (Stohl, 2002). As noted in the introduction, the mixing of pollution with time provides an upper limit on frequency for distant sources; only local sources can give a high frequency signal. The above-mentioned definitions are illustrated in **Figure 2**. One of the properties of diffusion is that a pulse of pollution will propagate in a Gaussian concentration profile depending on the diffusion constant and time. Under the Fourier transform, a Gaussian is mapped onto another Gaussian with a different width. The transform of a wide function is narrow and vice versa. By integrating periodograms in the three different frequency bins by the equations below, the relative contribution of local, urban and regional pollution of the LCS data can be quantified.

$$J_N(g) = \int_{\nu_{\text{start}}}^{\nu_{\text{end}}} g(\nu_k)\Phi(\nu_k)\,d\nu_k \tag{11}$$

Where ν_{start} and ν_{end} are the start and end frequencies in the chosen frequency bins, which is elaborated below:

$$\text{Regional}_N(g) = \int_0^{0.0139} g(\nu_k)\Phi(\nu_k)\,d\nu_k$$

$$\text{Urban}_N(g) = \int_{0.0139}^{0.0417} g(\nu_k)\Phi(\nu_k)\,d\nu_k$$

$$\text{Local}_N(g) = \int_{0.0417}^{0.5} g(\nu_k)\Phi(\nu_k)\,d\nu_k \tag{12}$$

and g is non-negative and square integrable with respect to Lebesgue measure on ν_k. After the relative contributions are calculated for each LCS node, the average concentration together with the standard deviation can be calculated across the AirNode network to illustrate how much local pollution the network is seeing on average and how much variation is seen across all AirNodes.

3 Results and discussion

In the following section we present the results of our study and of the data analysis.

3.1 Sensor data quality

230 The first requirement is to establish the fidelity of the monitoring network.

3.1.1 Missing data

The data completeness of the AirNodes varies between sites. In the monitoring network, apart from four AirNodes (4P04, 4P06, 4P08 and 4P20), all AirNodes have more than 80% data completeness during the sampling period. The four AirNodes with data completeness below 80% were excluded from the analysis. Across the network of AirNodes, the mean data completeness

235 is 95%, which is sufficient to investigate the local variation of air pollution. The main reasons for data gaps are the irregularities in the line power and lapses in the wireless internet connection. In addition, spiders had in a few cases entered through the small holes at the base of the AirNodes and nested in the housing leading to sensor failure.

3.1.2 Correction of NO$_2$ readings

It is necessary to account for temperature bias while deploying electrochemical NO$_2$ sensors (Alphasense, 2014). For our study,

240 this correction was crucial in order to get meaningful readings from the electrochemical sensors since the raw readings showed unphysical behavior. The typical NO$_2$ patterns during weekdays (Monday to Friday) and weekends (Saturday and Sunday) measured by AirNode4P01 as an example are shown before and after the correction in **Figure 3**. All AirNodes have the same tendencies, so **Figure 3** is characteristic of all AirNodes. For clarity, the NO$_2$_raw represents the Alphasense NO$_2$ cell output
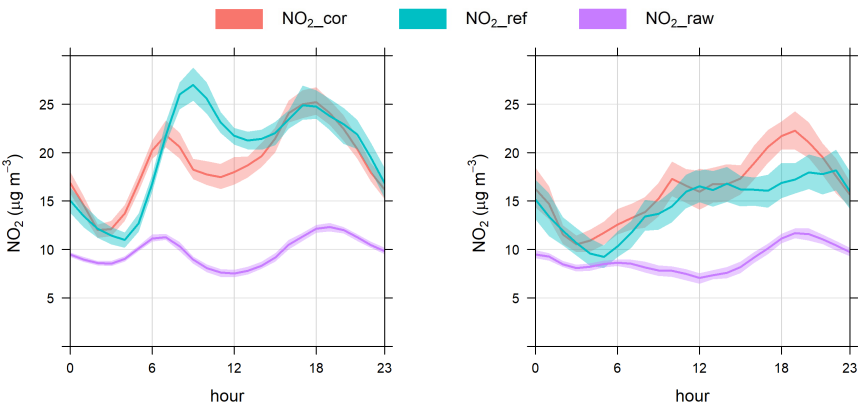
Figure 3. Daily patterns of NO$_2$ measured by the reference instrument (blue), corrected NO$_2$ concentrations (red) measured by one representative node (AirNode4P01) and uncorrected NO$_2$ concentrations (purple) measured by AirNode4P01 during weekdays (left) and weekends (right). Note the different scale y-axis. The shading shows the 95% confidence intervals of the mean. Please note that NO$_2$_raw represents the Alphasense NO$_2$ cell output (in dV) multiplied by the scale coefficient obtained from the laboratory calibration. The plots are produced by `timeVariation{openair}` (Carslaw, 2012).

(in dV) multiplied by the scale coefficient obtained from the laboratory calibration. The NO_2 patterns of the corrected NO_2
readings compared to the readings from the reference indicate that the correction procedure can overcome most of the disparity
between the readings during higher temperatures. Modeled temperature data from DEFRA (DEFRA, 2022) are used to correct
for the temperature bias. The correction coefficients for the AirNodes were calculated for each individual AirNode and the
mean and standard deviation of the correction coefficients are: a_0 = 20.83 (13.29), a_1 = -0.30 (0.17), a_2 = 1.37 (0.58), a_3 =
892.38 (521.02). All four terms in the linear regression model have a p-value of below 0.05 for all AirNodes. The relatively high
standard deviations are linked to the known intra-sensor variability and show that each sensor requires individual calibration
and/or correction. The correction coefficient, a_0, or offset of the sensor, is higher than the average concentration and it has
a relatively high standard deviation. This is a property of the Alphasense cell and can vary significantly from cell to cell,
which underscores the importance of calibrating and correcting the raw data from low-cost sensors in order to obtain accurate
concentrations.

It is known that in cities the temperature can vary strongly over small distances (Cao, 2021), therefore it would have been
more accurate to measure the internal temperature of the AirNodes and use that information for the correction. However, the
correction methodology even with the modeled temperature data, yields corrected readings that follow expected trends, giving
confidence in sensor accuracy. However, as seen in **Figure 3**, there is still a relatively large discrepancy between the reference
and the corrected AirNode readings on weekdays between 8 and 12 h, which can be attributed to the large distance between
the reference instrument and the AirNodes (4.1 km) and the fact that the concentration of NO_2 can have different profiles at
different locations, depending on the traffic modes and sources. Sensor performance is validated below.
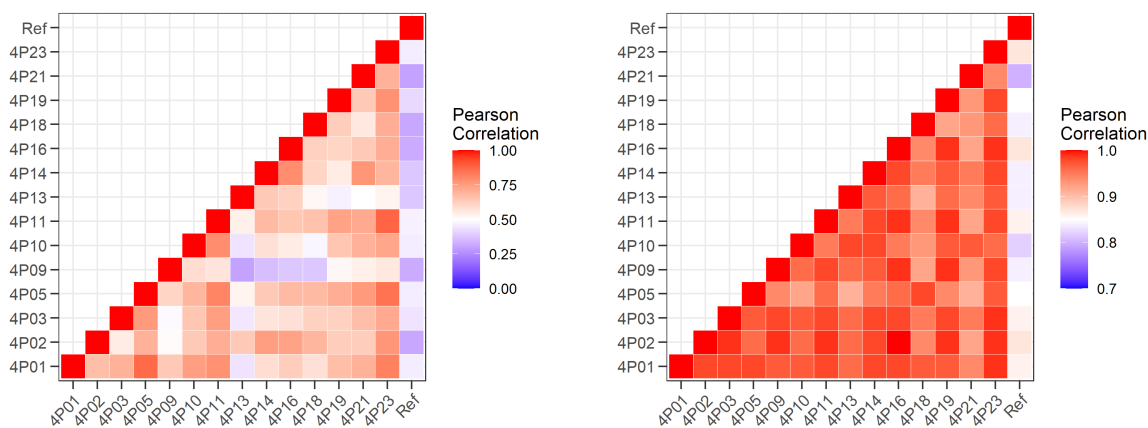
Figure 4. Correlation heatmap of Pearson correlation coefficient for NO_2 (left) and $PM_{2.5}$ (right). Note the different scales.

3.1.3 Inter-sensor variability

Inter-sensor variability has been used as a metric of sensor reliability in recent studies (Liu, 2020). **Figure 4** displays the correlation heatmap of Pearson correlation coefficient for NO_2 and $PM_{2.5}$, in which the respective reference measurements from Stoke-on-Trent Centre are included. The Pearson correlation coefficients for $PM_{2.5}$ among the AirNodes ranged from 0.87 to 0.99 with a mean of 0.95. In contrast, the Pearson correlation coefficients for NO_2 ranged from 0.30 to 0.88 with a mean of 0.64. For $PM_{2.5}$, the lowest Pearson correlation coefficients were above our quality criteria of 0.85. We did not choose a similar criterion for NO_2 since we expect there is much higher variation between the sensors due to localized sources. The AirNode network readings rose and fell simultaneously as ambient concentrations and conditions changed confirming that the sensors are operating as expected and giving confidence in sensor measurement reliability. The AirNode readings generally followed the same trends as seen at the reference instruments at Stoke-on-Trent Centre. The mean Pearson correlation coefficient for NO_2 was 0.40 with a range of 0.3 to 0.47, whereas the mean Pearson correlation coefficient for $PM_{2.5}$ was 0.85 with a range of 0.80 to 0.87. Again, the larger discrepancy between the reference and the corrected NO_2 readings can be attributed the more spatially variable nature of NO_2.

3.2 Descriptive statistics

Air quality data for NO_2 and $PM_{2.5}$ measured at the different sites during 2020 and 2021 were analyzed. For this section, only one year of data (August 1, 2020 to August 1, 2021) is used to compare with official guidelines. Descriptive statistics of the air quality measurements are presented in **Table 2**. The mean concentrations are compared to WHO's recently updated European AQGs and the legally binding EU standards, see **Table 1**. It should be noted that the legally binding values for annual means are defined for January, 1 to December, 31. The mean annual NO_2 and $PM_{2.5}$ concentrations across the network exceed the updated WHO guidelines by 7 and 3 $\mu g \ m^{-3}$ for NO_2 and $PM_{2.5}$, respectively. All sites have days where the daily average NO_2 and $PM_{2.5}$ concentrations exceed the WHO daily average AQG limits during the period. However, none of the sites are above the legally binding EU standards.

The values obtained from the network can be analyzed in relation to the values reported by AQMSs, as long as the significant distance between the measurement locations is kept in mind. The values from the network are compared with the three AQMSs: the monitoring station at Stoke-on-Trent A50 Roadside, the urban background monitoring station at Stoke-on-Trent Centre and the regional background monitoring station at Ladybower. Only the urban background station at Stoke-on-Trent Centre reported $PM_{2.5}$. Concentrations of NO_2 and $PM_{2.5}$ (when available) are averaged within the same period as the AirNodes in the network (i.e. August 1, 2020 to August 1, 2021), and the descriptive statistics are shown in **Table 2**. The mean concentrations obtained from the network show similar values for NO_2 and $PM_{2.5}$ as those seen at the urban background station. On average while the network sees lower NO_2 values than the roadside monitoring station (21.4 $\mu g \ m^{-3}$), there is an NO_2 excess relative to the regional background exposure (12.5 $\mu g \ m^{-3}$). In an environment such as a city with an elevated urban background concentration, exposure to air pollution in micro-environments can cause exceedance of recommended threshold values for many individuals in addition to the dangers of transient and continued exposure.

	NO$_2$ concentration (μg m^{-3})					PM$_{2.5}$ concentration (μg m^{-3})				
Sensor	Mean	Median	SD	Max	Exceedance[a]	Mean	Median	SD	Max	Exceedance[b]
AirNode4P01	18	16	11	82	41	9	5	12	122	58
AirNode4P02	17	11	12	101	45	7	4	8	101	26
AirNode4P03	18	15	11	89	44	9	6	10	121	40
AirNode4P05	17	16	10	78	37	8	4	10	109	42
AirNode4P09	19	16	13	91	51	8	4	11	119	44
AirNode4P10	19	18	10	100	36	10	5	15	241	54
AirNode4P11	18	17	10	71	36	11	6	13	125	43
AirNode4P13	17	11	13	100	34	7	4	9	94	27
AirNode4P14	17	10	13	91	60	7	4	9	92	19
AirNode4P16	15	10	11	89	34	8	5	10	132	27
AirNode4P18	17	14	11	86	43	7	4	11	163	33
AirNode4P19	18	16	11	95	38	6	3	8	89	33
AirNode4P21	18	15	10	83	47	7	4	11	140	32
AirNode4P23	18	16	10	77	30	9	5	13	129	56
Network mean	17.5	14.4	11.2	88.0	41.1	8.1	4.3	10.7	126.8	38.1
Network SD	0.9	2.5	1.0	9.1	7.9	1.4	0.9	1.9	38.6	12.1
Regional station	5	4	4	45	0	-	-	-	-	-
Urban station	19	16	13	102	64	8	6	7	74	6
Roadside station	39	35	25	155	271	-	-	-	-	-

[a] Number of days with an average NO$_2$ concentration above WHO's guideline of 25 μg m^{-3}

[b] Number of days with an average PM$_{2.5}$ concentration above WHO's guideline of 15 μg m^{-3}

Table 2. Statistics for air quality data measured from Aug 01, 2020 to Aug 01, 2021. For comparison, the descriptive statistics from the three regulatory air quality monitoring stations (Regional = Ladybower, urban background = Stoke-on-Trent Centre, roadside = Stoke-on-Trent A50 Roadside) are shown for the corresponding period. Neither Ladybower nor Stoke-on-Trent A50 Roadside has instruments for monitoring PM$_{2.5}$. Abbreviations: SD = standard deviation, max = maximum value. We are aware that the measurement uncertainty is significantly higher for low-cost air pollution sensors than for reference air quality monitoring measurements. However, EU air quality guidelines approve low-cost sensor data as indicative but not quantitative data - in line with calculations with air quality models.

3.3 Temporal trends

Figure 3 shows the temporal variation in NO$_2$. On weekdays, the NO$_2$ concentration increases in two time periods during the day, with peaks at 7:00 and 18:00. On weekends, the NO$_2$ concentration rises steadily throughout the day. There is a notable decrease in concentration during the weekend compared to the weekdays at all sites. For both weekends and weekdays the NO$_2$ concentration is lowest at night. The two time periods with increased NO$_2$ concentration during the weekdays are typically periods of increased traffic during morning and afternoon rush hours when people commute to and from work (Vignati, 1996;

Berkowicz, 1996). Thus, traffic likely drives this observed variation, in line with the declining NO$_2$ concentration during the night and over the weekend.

In terms of monthly trends, **Figure 5** displays the monthly average of the NO$_2$ concentration measured by one of the AirNodes together with the monthly readings from the nearest urban background AQMS (Stoke-on-Trent Center). All AirNodes have the same tendencies, so **Figure 5** is characteristic of all AirNodes. The readings from the AirNode and the AQMS follow the same trends, with the highest NO$_2$ concentrations in the Spring and the Winter.

3.4   Spatial trends

Wind speed and direction have been shown to provide essential information that can help identify source location (Carslaw, 2006; Westmoreland, 2007). The description of variation with wind direction and wind speed on a specific street (the so-called *street canyon effect*) is described in Berkowicz (1996). Bivariate polar plots are a powerful tool for source characterization including mean pollutant concentrations for specific wind speed and direction bins (Uria-Tellaetxe, 2012; Grange, 2016; Carslaw, 2012, 2013). In these plots wind direction is displayed from 0 to 360°clockwise on the angular axis and wind speed is shown on the radial scale.

The wind speed and direction data used in this study are shown as a windrose in **Figure 6**. The windrose shows that the prevailing winds come from the south and northwest during the measurement period. To assess spatially-resolved source patterns, bivariate polar plots of the NO$_2$ and PM$_{2.5}$ are investigated. The bivariate polar plots for each pollutant for all sites are shown in **Figure 7**. Reddish colors represent higher values compared to the blueish ones.
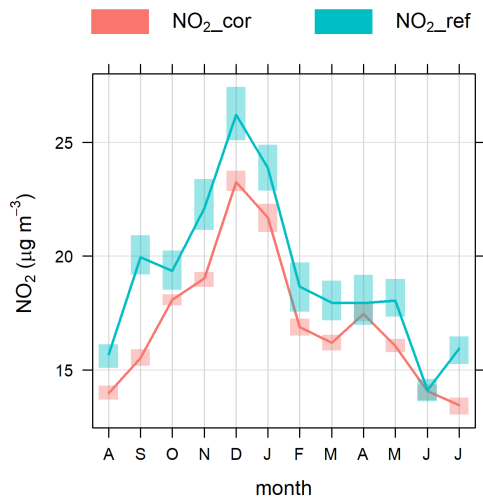
Figure 5. Monthly variation of NO$_2$ measured by one representative node (AirNode4P10) (red) and the corresponding reference instrument at Stoke-on-Trent Center (blue). The plot is produced by `timeVariation{openair}` (Carslaw, 2012).

The bivariate polar plots show patterns that depend on deployment location. AirNode4P23, AirNode4P19 and AirNode4P02 are located in the southern part of the ring road, and they display similar patterns in their bivariate polar plots. Their surroundings are almost identical and the traffic influence on their readings is similar. The nodes located in the northern part of the ring road have different patterns relative to the ones in the southern area. They experience the highest values at lower wind speeds. When peak concentrations occur at low wind speeds it suggests local sources. For example in a street canyon there is both a direct and a recycled contribution to the concentration, where the relative size of these two contributions depends on whether the measuring site at a given time is in the leeward or windward side of the street. AirNode4P10 is located in front of a school, and at lower wind speeds or with westerly wind, elevated levels of NO_2 were observed. In general, the highest concentrations are observed at low wind speeds, where no whirlwind is formed inside the street, independent of wind directions, or when the measuring site is on the leeward side of the street (in relation to the whirlwind). In the latter case, pollution from the traffic in the specific section of the street will be led directly to the measuring site, at the same time as there is a contribution due to trapping of pollution within the limited volume of the whirlwind.

Higher NO_2 values are correlated with wind speed and the orientation of the road. The traffic comes from the ring road area and continues through St. Paul's Road. Near the school, traffic stops frequently and accelerates and idles while children are being dropped off and picked up. The lowest values of NO_2 are seen at higher wind speeds with northwesterly winds. The bivariate polar plot for AirNode4P01 and AirNode4P05 show similar patterns, with the highest concentrations found for easterly and southwesterly winds, whereas the lowest concentrations were seen with westerly and southwesterly winds. Higher
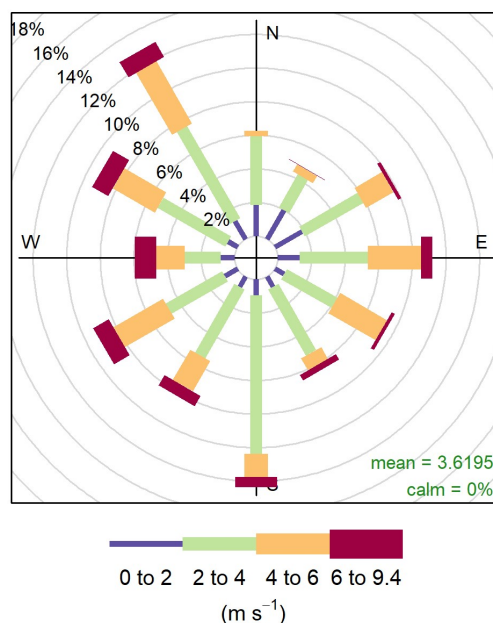
Figure 6. Windrose showing the frequency of counts by wind direction (%). The plot is produced by `windRose{openair}` (Carslaw, 2012).

335 speed southwesterly winds contributed to the peak concentrations at these locations. A wide-open parking area is located next to the ring road in that direction, which could explain the elevated concentrations.
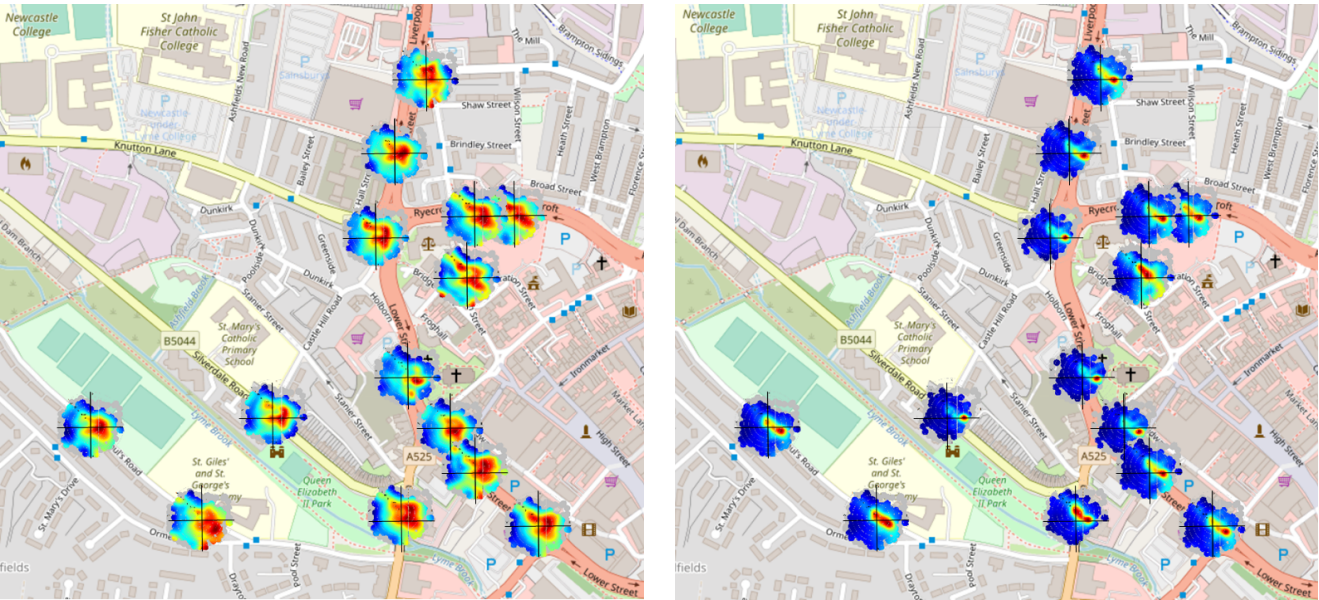
Figure 7. Bivariate polar plots of NO_2 (left) and $PM_{2.5}$ (right) show the spatial variability in the study area for the entire study period. The figures are produced by `polarMap{openairmaps}` (`openairmaps` is a package that supports `openair` (Carslaw, 2012) for plotting on various maps), where the maps are obtained from ©OpenStreetMap contributors 2021. Distributed under the Open Data Commons Open Database License (ODbL) v1.0 (OpenStreetMap, 2021).

The wind speed dependence of concentrations in a street canyon can be complex as there are opposing effects: Higher wind speeds lead to more O_3 but also more dilution of NO_x (NO + NO_2). High wind speeds will therefore lead to lower NO_2 while at low wind speeds, NO_2 formation is limited by O_3, which goes towards zero in the street (Palmgren, 1996). Bivariate polar

340 plots are good at revealing these interrelationships. The wind speed dependence can help distinguish sources from one another. When several measurement sites are available, polar plots can triangulate different sources (Carslaw, 2006). As expected, NO_2 is dominated by local emissions, and peak values mainly occur for low wind speeds, where elevated concentrations were observed due to accumulation and lack of dispersion. The most obvious features of NO_2 bivariate polar plots are that the elevated levels are attributable to the orientation of the road or the place with the highest traffic density.

345 Relative to the bivariate polar plots of NO_2, the bivariate polar plots of $PM_{2.5}$ do not show as much variation across the network. Generally, the highest concentrations of $PM_{2.5}$ are seen for southeasterly winds and higher wind speeds. This is confirmed by the frequency spectrum showing slow changes consistent with large air masses. This indicates that particles originate from long-range transport. The bivariate polar plots for $PM_{2.5}$ also suggest that the locally-sourced particulate matter is present, shown by the elevated concentrations at low wind speeds, where the atmospheric conditions are more stable.
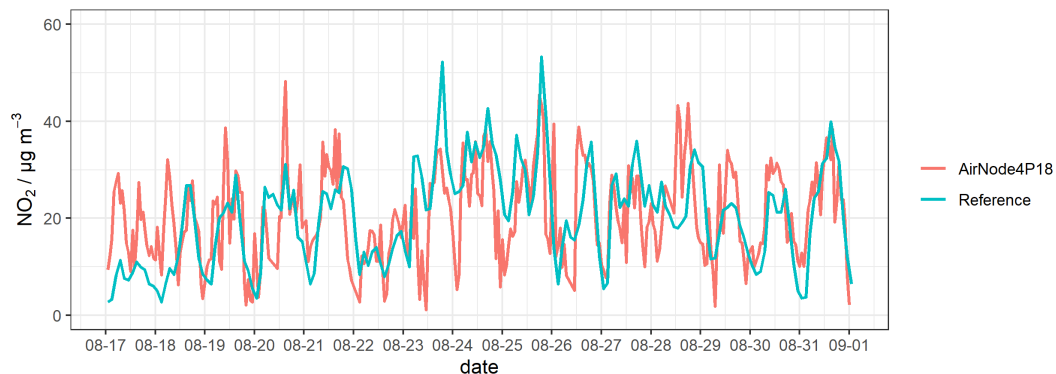
Figure 8. Time series of NO$_2$ measured by one representative AirNode (AirNode4P18) with a time-resolution of 30 minutes and the corresponding reference instrument at Stoke-on-Trent Center with a time-resolution of 1 hour. For clarity, only two weeks of data are shown.

350   In general, sites across the sensor network show a variation in their bivariate polar plots (however more for NO$_2$ than for PM$_{2.5}$) due to the different pollution sources. Thus, there are additional benefits of multi-sensor node measurements for characterizing sources in detail, especially when combining them with meteorological information.

    Figure 8 shows data from the urban background AQMS at Stoke-on-Trent Centre at a time-resolution of 1 hour (DEFRA, 2022). Data from one of the AirNodes with a time-resolution of 30 minutes is shown for comparison. The raw readings from the
355 AirNodes have a time-resolution of 1 minute, however, the temperature correction aggregates the data into 30 minute bins. Still, with a time-resolution of 30-minutes, we see more local variability in the data, compared to the readings from the reference station. The data have a measurement density in both time and space, which can not be achieved using current conventional measurement methods. As seen on **Figure 8**, the readings from the AirNode and the AQMS follow the same trend, but the correlation of determination is only 0.28. This is expected since the AQMS is located around 4 km from the AirNode network.
360 However, increasing the time-resolution will increase the correlation of determination, i.e., a time-resolution of 3 hours results in a correlation of determination of 0.38, and a time-resolution of 1 day yields 0.63.

3.5 Spectral analysis

Spectral analysis is performed on the air pollution data to investigate its hidden periodicities and quantify their magnitude. The contributions of local and regional sources to the pollution concentrations are determined based on the determined amplitudes
365 and frequencies. The local sources are shown in the high-frequency periodogram, and the regional or long-range sources are revealed in the low-frequency periodogram. Note however that local sources may be present in both the low and high frequency regions. For example, in an urban street, the traffic patterns follow stable patterns with daily and weekly periodicities. Holiday periods follow their own pattern, and for wood smoke, emissions follow variations in outdoor temperature. By comparing the spectra for the different pollutants measured by the same AirNode, information on the sources can be revealed. If the emission
370 sources for the different pollutants are the same, similarly cyclic patterns can be expected. The differences in the pollution
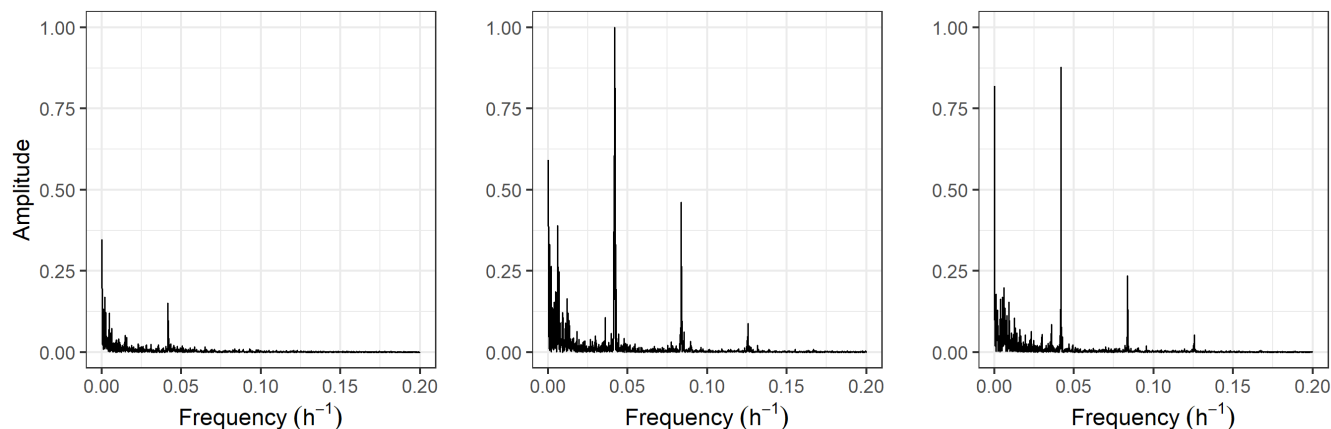
Figure 9. Periodograms for NO_2 at regional background AQMS, Ladybower (left), street AQMS, Stoke-on-Trent A50 Roadside (middle) and urban background AQMS, Stoke-on-Trent Centre (right). All periodograms are normalized against the highest peak.

spectra can indicate a contribution from the different pollutant sources or the presence of chemical transformation since all other conditions are identical.

Spectral analysis is performed on NO_2 data from three different types of AQMSs to illustrate how periodograms vary depending on location. These AQMSs are 1) regional background (Ladybower), 2) urban background (Stoke-on-Trent Centre) and 3) street (Stoke-on-Trent A50 Roadside). The three periodograms are shown in **Figure 9**. While all three periodograms have significant peaks in the low-frequency region, only the urban background and street AQMSs have significant peaks in the high-frequency region. We conclude that these high frequency peaks are due to the proximity and strength of local NO_2 sources.
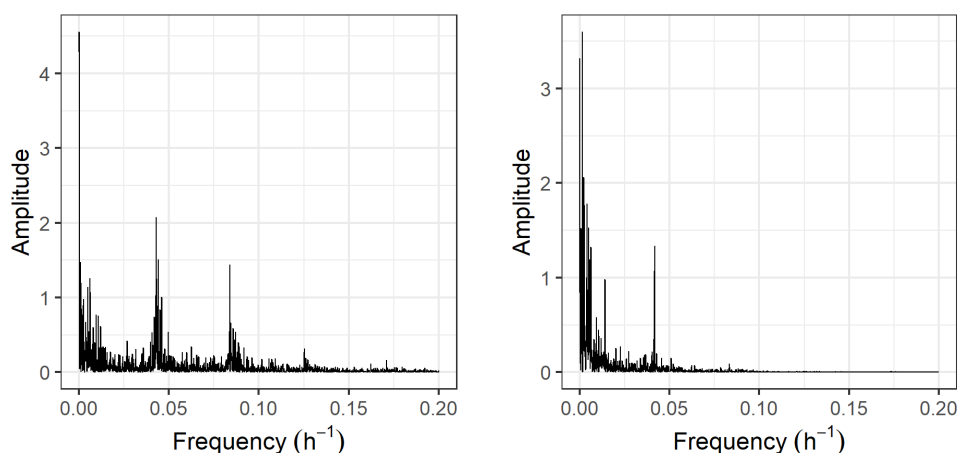
Figure 10. Periodogram of NO_2 (left) and $PM_{2.5}$ (right) obtained by AirNode4P01.

Figure 10 displays the periodograms for NO_2 and $PM_{2.5}$ measured by AirNode4P01. The periodogram of NO_2 features three distinct peaks at 0.125, 0.084 and 0.042 h^{-1} corresponding to periods of 8, 12 and 24 h, respectively. In addition, one peak is identifiable in the high-frequency region at 0.17 h^{-1} (6 h). In the low-frequency region, there are multiple peaks close to each other, however, the peaks corresponding to 5 days (0.0083 h^{-1}), 1 week (0.0061 h^{-1}) and 1 month (0.00135 h^{-1}) can still be identified. All these cycles can be related to local sources of pollution e.g. traffic or meteorological changes. Peaks located in the low-frequency region can originate from changes over either synoptic or larger scale. Highest intensity occurs in the high-frequency region since most of NO_2 originates from local sources. The daily changes in NO_2 concentrations can be associated with the daily changes in traffic from nearby roads and the diurnal variation caused by sunlight. Weekly periodicity may also originate from changes in traffic.

The periodogram for $PM_{2.5}$ (see **Figure 10**) features one distinct peak in the high-frequency region at 0.042 h^{-1} (24 h), and a prominent peak at 0.084 h^{-1} (12 h). Besides these two peaks, most peaks are seen in the low-frequency region of the periodogram, which is expected since $PM_{2.5}$ is dominated by long-range transport and non-local sources. However, the contribution by PM from a nearby road can originate from traffic since vehicles, in general, can re-suspend particles from the road into the air, and abrasion from brakes and tires also produce PM (Grigoratos, 2015).

Periodograms for the rest of the AirNodes in the network show results similar to the ones shown in **Figure 10**, with small changes in position and amplitude at specific locations. Conclusions regarding trends in pollution sources can be drawn by examining the relative contributions from local, urban and regional sources. **Figure 11** shows the calculated percentages of local, urban and regional contributions for the AirNodes as well as for the three different types of AQMSs. The results for the network indicate that local emissions are the most important source of NO_2 with an average of 54.3 ± 4.3 %, whereas $PM_{2.5}$ is mainly due to regional sources (62.1 ± 3.5 %). For NO_2, urban sources contribute 14.3 ± 1.9 % and regional sources 31.2 ± 4.5 %. For $PM_{2.5}$, urban sources contribute 20.0 ± 1.2 % and local sources 17.9 ± 3.2 %.

As expected the regional background AQMS shows the highest relative contribution from of regionally sourced NO_2, and the street AQMS has the highest level of locally sourced NO_2. The AirNodes in the network show a distribution of contributions.

The results obtained for both NO_2 and $PM_{2.5}$ reveal contributions of short-term (12 h and 24 h) and long-term fluctuations. The contributions at low frequencies are significantly different between the two pollutants, indicating that temporal variations are influenced by different processes. The methodology is a powerful tool for analyzing the causes of air pollution.

4   Conclusions

Air pollution can be hyper-local and low-cost air pollution sensors are capable of accurately describing variation close to pollution sources. This study assessed more than one year of NO_2 and $PM_{2.5}$ data with high spatiotemporal resolution (1-min) obtained using a network of 18 low-cost air pollution sensor nodes. Initially there were significant calibration issues associated with temperature bias in the NO_2 readings but a simple and effective temperature, scale and offset correction was able to overcome this problem. Therefore, this study, like many others, clearly indicates that while low-cost air pollution sensors can be useful, calibration and correction is far from trivial and requires supporting data from reference stations. The corrected NO_2

In its recent update and revision of the air quality guidelines for Europe, the WHO has proposed annual NO_2 and $PM_{2.5}$ exposure guideline thresholds of 10 and 5 $\mu g\ m^{-3}$, respectively. The annual mean NO_2 and $PM_{2.5}$ concentrations across the network exceed the updated WHO guidelines by 7 $\mu g\ m^{-3}$ for NO_2 and 3 $\mu g\ m^{-3}$ for $PM_{2.5}$. However, none of the sites had values exceeding the legally binding UK/EU standards. An excess concentration of 12.5 $\mu g\ m^{-3}$ of NO_2 in the network was seen relative to background levels measured by the regional monitoring station at Ladybower reservoir. This highlights the risk of pollution exposure for individuals due to local sources and supports the use of local monitoring to characterize the risk.
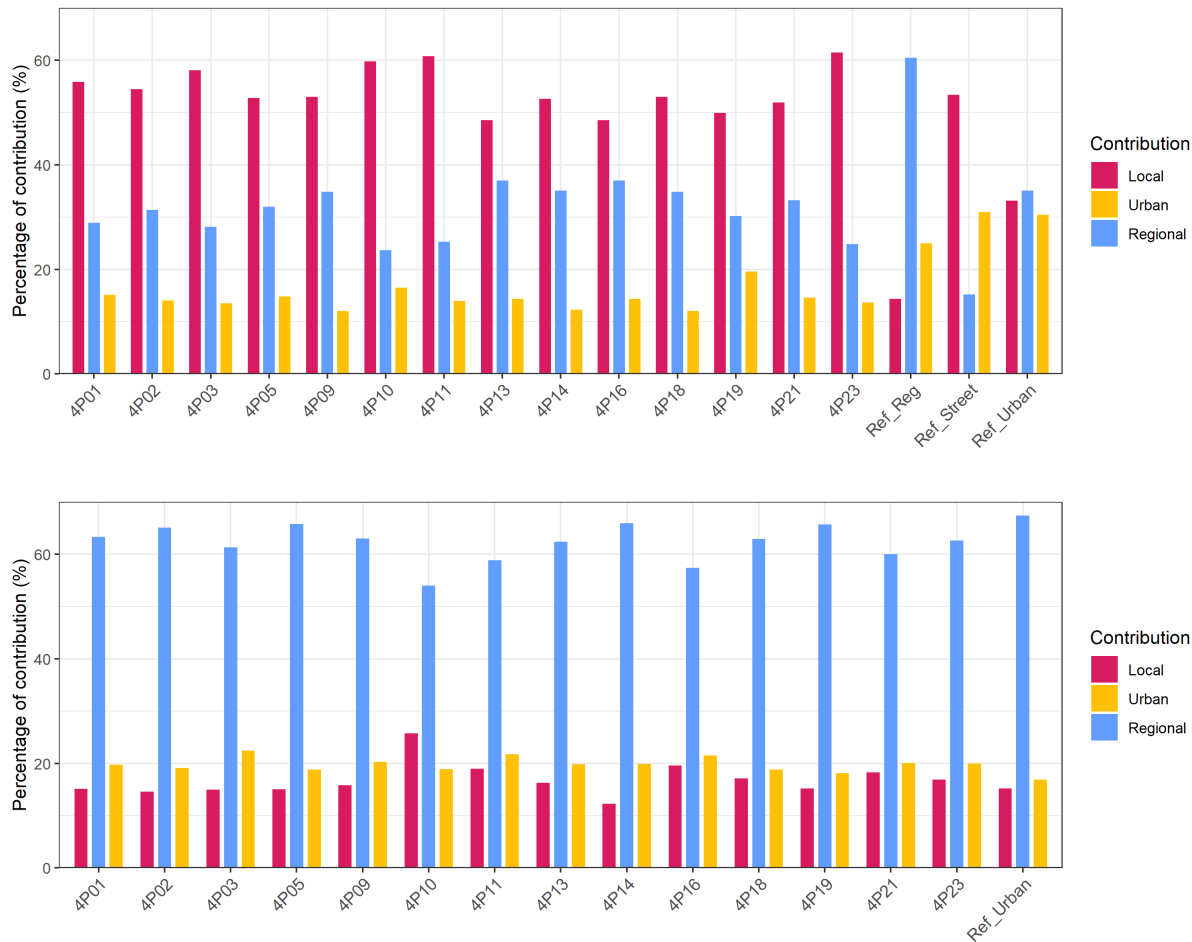
Figure 11. Histogram of percentages of contribution (%) of local (red), urban (yellow) and regional sources (blue) for NO_2 (top) and $PM_{2.5}$ (bottom) measured by all AirNodes in the network as well as for the three AQMS. *Ref_Reg* is the regional background AQMS, Ladybower, *Ref_Street* is the street AQMS, Stoke-on-Trent A50 Roadside, and *Ref_Urban* is the urban background AQMS, Stoke-on-Trent Centre.

420   Spectral analysis is found to be a good method for studying the variation within the time series. This approach enabled the detection of different underlying periodicities in time series data and allowed the pollution signal to be apportioned to different categories of pollution source whether local, urban or regional. The results highlighted the advantages of having a densely deployed sensor network over the sparse conventional air quality monitoring stations. The highly increased spatio-temporal resolution of low cost sensors combined with their dense placement near pollution sources makes it possible to

425 provide additional information on the patterns and sources of air pollution, which in turn provides a better description of the highly variable and complex nature of pollution.

Data availability. All raw data is available upon request

Author contributions. Conceptualization: MSJ, JAS, LBF. Methodology: LBF, MSJ, JAS. Software: JAS, RS. Validation: LBF, RS, JAS. Formal analysis: LBF. Investigation: LBF. Resources: MSJ. Data curation: LBF. Writing–original draft preparation: LBF. Writing–review and
430 editing: LBF, MSJ, RS, JAS, OH. Visualization: LBF. Supervision: JAS, OH, MSJ. Project administration: MSJ, JAS. Funding acquisition: MSJ, OH.

Competing interests. RS, JAS and MSJ are employees of AirLabs and LBF is partly funded by AirLabs.

Acknowledgements. The authors thank Bartosz Gaik and Archie Waller for their dedicated and professional assistance with logistical and technical issues. The authors acknowledge ©OpenStreetMap contributors 2021 for map data, available from https://www.openstreetmap.org,
435 and David Carslaw for providing the online available `openair` package in R. LBF is supported by BERTHA - the Danish Big Data Centre for Environment and Health funded by the Novo Nordisk Foundation Challenge Programme (grant NNF17OC0027864).

References

Abdo, N., Khader, Y.S., Abdelrahman, M., Graboski-Bauer, A., Malkawi, M., Al-Sharif, M. and Elbetieha, A. M.: Respiratory health outcomes and air pollution in the Eastern Mediterranean Region: a systematic review. Environ. Health Rev., 31, 2, 259-280, https://doi.org/10.1515/reveh-2015-0076, 2016

Ai, S., Wang, C., Qian, Z.M., Cui, Y., Liu, Y., Acharya, B. K., Sun, X., Hinyard, L., Jansson, D. R., Qin, L. and Lin, H.: Hourly associations between ambient air pollution and emergency ambulance calls in one central Chinese city: Implications for hourly air quality standards. Sci. Total Environ., 696, 133956, https://doi.org/10.1016/j.scitotenv.2019.133956, 2019

Alphasense. Alphasense application note 803: Correcting for background currents in four electrode toxic gas sensors. Technical report, AAN 803-01, Alphasense Ltd, https://zueriluft.ch/makezurich/AAN803.pdf, 2014.

Alphasense Ltd: Technical specification NO_2 Sensor, NO2-B43F Nitrogen Dioxide Sensor 4-electrode. Version V1. Data sheet, https://www.alphasense.com/wp-content/uploads/2019/09/NO2-B43F.pdf, 2019

Berkowicz, R., Palmgren, F., Hertel, O., and Vignati, E.: Using measurements of air pollution in streets for evaluation of urban air quality - meteorological analysis and model calculations. Sci. Total Environ., 189/190, 259-265, http://dx.doi.org/10.1016/0048-9697(96)05217-5, 1996

Borrego, C., Costa, A. M., Ginja, J., Amorim, M., Coutinho, M., Karatzas, K., Sioumis, Th., Katsifarakis, N., Konstantinidis, K., De Vito, S., Esposito, E., Smith, André, N., Gérard, P., Francis, L.A., Castell, N., Schneider, P., Viana, M., Minguillón, M. C., Reimringer, W., Otjes, R. P., von Sicard, O., Pohle, R., Elen, B., Suriano, D., Pfister, V., Prato, M., Dipinto, S. and Penza, M.: Assessment of air quality microsensors versus reference methods: The EuNetAir joint exercise. Atmos. Environ., 147, 246-263, https://doi.org/10.1016/j.atmosenv.2016.09.050, 2016

Brasseur, G. and Jacob, D. Modeling of Atmospheric Chemistry. Cambridge: Cambridge University Press. https://doi:10.1017/9781316544754, 2017

Budde, M. and Schwarz, A.D and Müller, T. and Laquai, B. and Streibl, N. and Schindler, G. and Köpke, M. and Riedel, T. and Dittler, A. and Beigl, M.: Potential and limitations of the low-cost SDS-011 particle sensor for monitoring urban air quality. ProScience, 5, 6–12, https://doi:10.14644/dust.2018.002, 2018

Bulot, F. M. J., Russell, H. S., Rezaei, M., Johnson, M. S., Ossont, S. J. J., Morris, A. K. R., Basford, P. J., Easton, N. H. C., Foster, G. L., Loxham, M. and Cox, S. J.: Laboratory comparison of low-cost particulate matter sensors to measure transient events of pollution. Sensors, 20, 8, 2219, https://doi.org/10.3390/s20082219, 2020

Cao, J. and Zhou, W. and Zheng, Z. and Ren, T. and Wang, W.: Within-city spatial and temporal heterogeneity of air temperature and its relationship with land surface temperature, Landsc Urban Plan, 206, https://doi.org/10.1016/j.landurbplan.2020.103979, 2021

Carslaw, D. C., Beevers, S. D., Ropkins, K. and Bell, M. C. Detecting and quantifying the contribution made by aircraft emissions to ambient concentrations of nitrogen oxides in the vicinity of a large international airport. Atmos. Environ., 40, 28, 5424–5434, https://doi.org/10.1016/j.atmosenv.2006.04.062, 2006

Carslaw, D. C. and Ropkins, K.: *openair* — An R package for air quality data analysis. Environ. Model. Softw., 27-28, 52-61, https://doi.org/10.1016/j.envsoft.2011.09.008, 2012

Carslaw, D. C. and Beevers, S. D.: Characterising and understanding emission sources using bivariate polar plots and k-means clustering. Environ. Model. Softw., 40, 325-329, https://doi.org/10.1016/j.envsoft.2012.09.005, 2013

Castell, N., Dauge, F. R., Schneider, P., Vogt, M., Lerner, Uri., Fishbain, B., Broday, D. and Bartonova, A.: Can commercial low-cost sensor platforms contribute to air quality monitoring and exposure estimates?. Environ. Int., 99, 293-302, https://doi.org/10.1016/j.envint.2016.12.007, 2017

Chen, G., Guo, Y., Abramson, M.J., Williams, G. and Li, S.: Exposure to low concentrations of air pollutants and adverse birth outcomes in Brisbane, Australia, 2003–2013. Sci. Total Environ., 622, 721-726, https://doi.org/10.1016/j.scitotenv.2017.12.050, 2018

Choi, Y.-S., Ho, C.-H., Chenb, D., Noha, Y.-H., and Song, C.-K.: Spectral analysis of weekly variation in PM_{10} mass concentration and meteorological conditions over China. Atmos. Environ., 42, 655–666, https://doi.org/10.1016/j.atmosenv.2007.09.075, 2008

Cross, E.S. and Williams, L.R. and Lewis, D.K. and Magoon, G.R. and Onasch, T.B. and Kaminsky, M.L. and Worsnop, D.R. and Jayne, J.T.: Use of electrochemical sensors for measurement of air pollution: Correcting interference response and validating measurements. Atmos. Meas. Tech., 10, 3575, https://doi.org/10.5194/amt-10-3575-2017, 2017

DEFRA (Department for Environment, Food and Rural Affairs). 2022.

Dey, A: Semiconductor metal oxide gas sensors: A review. MSEB, 229, 206–217, http://doi.org/10.1016/j.mseb.2017.12.036, 2018

Ellermann, T., Nygaard, J., Nøjgaard, J. K., Nordström, C., Brandt, J., Christensen, J. H., Ketzel, M., Massling, A., Bossi, R., Frohn, L. M., Geels, C., Jensen, S. S.: The Danish Air Quality Monitoring Programme: Annual Summary for 2018. Aarhus: Aarhus Universitet, 2020, p. 83 (Scientific Report from DCE – Danish Centre for Environment and Energy; Nr. 360).

The European Environment Agency: Europe's Environment - The Dobris Assessment. Chapther 4: Air. 2008. Retrieved from: https://www.eea.europa.eu/publications/92-826-5409-5/page004new.html (2008)

Eskridge, R., Ku, J. Y., Rao, S. T., Porter, P. S. and Zurbenko, I. G.: Separating different time scales of motion in time series of meteorological variables. Bull. Am. Meteorol. Soc., 78, 1473– 1483, https://doi.org/10.1175/1520-0477(1997)078<1473:SDSOMI>2.0.CO;2, 1997

Fine, G. F. and Cavanagh, L. M. and Afonja, A. and Binions, R.: Metal oxide semi-conductor gas sensors in environmental monitoring. Sensors, 10, 6, 5469–5502, https://doi.org/10.3390/s100605469, 2010

Fluharty, M., Bu, F., Steptoe, A. and Fancourt, D.: Coping strategies and mental health trajectories during the first 21 weeks of COVID-19 lockdown in the United Kingdom. Soc. Sci. Med., 279, 113958, https://doi.org/10.1016/j.socscimed.2021.113958, 2021

Frederickson, L.B., Lim, S., Russell, H.S., Kwiatkowski, S., Bonomaully, J., Schmidt, J.A., Hertel, O., Mudway, I., Barratt, B. and Johnson, M. S: Monitoring excess exposure to air pollution for professional drivers in London using low-cost sensors. MDPI Atmosphere, 11, 749, https://doi.org/10.3390/atmos11070749, 2020a

Frederickson, L. B., Petersen-Sonn, E. A., Yuwei, S., Hertel, O., Hong, Y., Schmidt, J. A. and Johnson, M. S.: Low-Cost Sensors for Indoor and Outdoor Pollution. Air Pollution Sources, Statistics and Health Effects. Springer US, New York, 423-453, 2020b

Gemmer, M. and Bo, X.: Air quality legislation and standards in the European Union: Background, status and public participation. Adv. Clim. Change Res., 4, 50-59, https://doi.org/10.3724/SP.J.1248.2013.050, 2013

Genikomsakis, K.N. and Galatoulas, N.-F. and Dallas, P.I. and Candanedo Ibarra, L.M. and Margaritis, D. and Ioakimidis, C.S.: Development and on-field testing of low-cost portable system for monitoring $PM_{2.5}$ concentrations. Sensors. 18, 1056–1072, https://doi:10.3390/s22072767 2018

Grange, S. K. and Lewis, A. C. and Carslaw, D. C.: Source apportionment advances using polar plots of bivariate correlation and regression statistics. Atmos. Environ., 145, 128-134, https://doi.org/10.1016/j.atmosenv.2016.09.016, 2016

Grigoratos, T. and Giorgio, M.: Brake wear particle emissions: A review. ESPR, 22, 4, 2491–504, https://doi:10.1007/s11356-014-3696-8, 2015

510 Heimann, I., Bright, V. B., McLeod, M. W., Mead, M. I., Popoola, O. A. M., Stewart, G. B. and Jones, R. L.: Source attribution of air pollution by spatial scale separation using high spatial density networks of low cost air quality sensors. Atmos. Environ., 113, 10-19, https://doi.org/10.1016/j.atmosenv.2015.04.057, 2015

Hertel, O., Ellermann, T., Palmgren, F., Berkowicz, R., Løfstrøm, P., Frohn, L. M., Geels, C., Ambelas Skjøth, C., Brandt, J., Christensen, J., Kemp, K., and Ketzel, M.: Integrated air pollution monitoring - combined use of measurements and models in monitoring programmes.
515 Environ. Chem., 4, 2, 65-74, http://dx.doi.org/10.1071/EN06077, 2007

Hies, T., Treffeisen, R., Sebald, L. and Reimer, E.: Spectral analysis of air pollutants. Part 1: elemental carbon time series. Atmos. Environ., 34, 3495-3502, https://doi.org/10.1016/S1352-2310(00)00146-1, 2000

Hogrefe, C., Porter, P. S., Gego, E., Gilliland, A., Gilliam, R., Swall, J., Irwin, J. and Rao, S. T.: Temporal features in observed and simulated meteorology and air quality over the Eastern United States. Atmos. Environ., 40, 5041–5055,
520 https://doi.org/10.1016/j.atmosenv.2005.12.056, 2006

Hwang, C. and Chen, S.-A.: Fourier and wavelet analyses of TOPEX/Poseidon-derived sea level anomaly over the South China Sea: A contribution to the South China Sea Monsoon Experiment. J. Geophys. Res., 105, 28785-28804, https://doi.org/10.1029/2000JC900109, 2000

IPCC: Masson-Delmotte, V., Zhai, P., Pirani, A., Connors, S. L., Péan, C., Berger, S., Caud, N., Chen, Y., Goldfarb, L., Gomis, M. I., Huang,
525 M., Leitzell, K., Lonnoy, E., Matthews, J. B. R., Maycock, T. K., Waterfield, T., Yelekçi, O., Yu, R. and Zhou, B. (eds.).: Climate Change 2021: The Physical Science Basis. Contribution of Working Group I to the Sixth Assessment Report of the Intergovernmental Panel on Climate Change. Cambridge University Press. 2021

Kingham, S., Briggs, D., Elliott, P., Fischer, P., and Lebret, E.: Spatial variations in the concentrations of traffic-related pollutants in indoor and outdoor air in Huddersfield, England. Atmos. Environ., 34(6), 905-916, https://doi.org/10.1016/S1352-2310(99)00321-0, 2000

530 Korotcenkov, G.: The role of morphology and crystallographic structure of metal oxides in response of conductometric-type gas sensors. Mater. Sci. Eng. R Rep., 61, 1, 1–39, https://doi.org/10.1016/j.mser.2008.02.001, 2008

Kumar, P., Morawska, L., Martani, C., Biskos, G., Neophytou, M., Di Sabatino, S., Bell, M., Norford, L. and Britter, R.: The rise of low-cost sensing for managing air pollution in cities. Environ. Int., 75, 199-205, https://doi.org/10.1016/j.envint.2014.11.019, 2015

Lazić, L., Urošević, M. A., Mijić, Z., Vuković, G. and Ilić, L.: Traffic contribution to air pollution in urban street
535 canyons: Integrated application of the OSPM, moss biomonitoring and spectral analysis. Atmos. Environ., 141, 347-360, https://doi.org/10.1016/j.atmosenv.2016.07.008, 2016

Lebret, E., Briggs, D., Van Reeuwijk, H., Fischer, P., Smallbone, K., Harssema, H., Kriz, B., Gorynski, P. and Elliott, P.: Small area variations in ambient NO2 concentrations in four European areas. Atmos. Environ., 34, 177-185, https://doi.org/10.1016/S1352-2310(99)00292-7, 2000

540 Lelieveld, J., Evans, J. S., Fnais, M., Giannadaki, D. and Pozzer, A.: The contribution of outdoor air pollution sources to premature mortality on a global scale. Nature. 525, 367–414, https://doi.org/10.1038/nature15371, 2015

Lewis, A. C., Lee, J. D., Edwards, P. M., Shaw, M. D., Evans, M. J., Moller, S. J., Smith, K. R., Buckley, J. W., Ellis, M. and Gillot, S. R.: Evaluating the performance of low cost chemical sensors for air pollution research. Faraday Discuss., 189, 85-103, https://doi.org/10.1039/C5FD00201J, 2016

545 Li, C., Wang, Z., Li, B., Peng, Z. R. and Fu, Q.: Investigating the relationship between air pollution variation and urban form. Build. Environ., 147, 559-568, https://doi.org/10.1016/j.buildenv.2018.06.038, 2019

Li, J., Hauryliuk, A., Malings, C., Eilenberg, S. R., Subramanian, R. and Presto, A. A.: Characterizing the aging of Alphasense NO_2 sensors in long-term field deployments. ACS Sens., 6, 8, 2952-2959 https://doi.org/10.1021/acssensors.1c00729, 2021

Liu, X., Jayaratne, R., Thai, P., Kuhn, T., Zing, I., Christensen, B., Lamont, R., Dunbabin, M., Zhu, S., Gao, J., Wainwright D., Neale, D., Kan, R., Kirkwood, J. and Morawska, L.: Low-cost sensors as an alternative for long-term air quality monitoring. Environ. Res., 185, https://doi.org/10.1016/j.envres.2020.109438, 2020

Liu, H.-Y. and Schneider, P. and Haugen, R. and Vogt, M.: Performance assessment of a low-cost $PM_{2.5}$ sensor for a near four-month period in Oslo, Norway. Atmosphere, 10, 411–59, https://doi.org/10.3390/atmos10020041, 2019

Lyons, T. J.: Mesoscale wind spectra, Q. J. R. Meteorol. Soc., 101, 901–910, https://doi.org/10.1002/qj.49710143013,1975

Maag, B., Zhou, Z. and Thiele, L.: A survey on sensor calibration in air pollution monitoring deployments, IEEE Internet Things J., 4857-4870, https://doi.org/10.1109/JIOT.2018.2853660, 2018

Marr, L. and Harley, R.: Spectral Analysis of Weekday–Weekend Differences in Ambient Ozone, Nitrogen Oxide, and Non-methane Hydrocarbon Time Series in California. Atmos. Environ., 36, 2327-2335, https://doi.org/10.1016/S1352-2310(02)00188-7, 2002

Mead, M., Popoola, O., Stewart, G., Landshoff, P., Calleja, M., Hayes, M., Baldovi, J., McLeod, M., Hodgson, T., Dicks, J., Lewis, A. C., Cohen, J., Baron, R., Saffell, J. and Jones, R.: The use of electrochemical sensors for monitoring urban air quality in low-cost, high-density networks. Atmos. Environ., 70, 186-203, https://doi.org/10.1016/j.atmosenv.2012.11.060, 2013

Monn, C.: Exposure assessment of air pollutants: a review on spatial heterogeneity and indoor/outdoor/personal exposure to suspended particulate matter, nitrogen dioxide and ozone. Atmos. Environ., 35, 1-32, https://doi.org/10.1016/S1352-2310(00)00330-7, 2001

Motlagh, N. H., Lagerspetz, E., Nurmi, P., Li, X., Varjonen, S., Mineraud, J., Siekkinen, M., Rebeiro-Hargrave, A., Hussein, T. and Petaja, T: Toward massive scale air quality monitoring. IEEE Commun. Mag., 58, 2, 54-59, https://doi.org/10.1109/MCOM.001.1900515, 2020

Narayanan, V. A. and Prabhu, K. M. M.: The fractional Fourier transform: Theory, implementation and error analysis. Microprocess Microsyst, 27, 10, 511-521, https://doi.org/10.1016/S0141-9331(03)00113-3, 2003

OpenStreetMap contributors. Retrieved from: https://www.openstreetmap.org (2021). Copyright: https://www.openstreetmap.org/copyright

Palmgren, F., Berkowicz, R., Hertel, O., and Vignati, E.: Effects of reduction in NO_x on the NO_2 levels in urban streets. Sci. Total Environ., 189/190, 409-415, http://dx.doi.org/10.1016/0048-9697(96)05238-2, 1996

Parseval, M.-A.:Mémoire sur les séries et sur l'intégration complète d'une équation aux différences partielles linéaires du second ordre, à coefficients constants. Mém. prés. par divers savants, Acad. des Sciences, Paris,(1), 638-648, 1806

Percival, D. and Walden, A.: Spectral analysis for physical applications. Cambridge University Press, https://doi.org/10.1017/CBO9780511622762, 1998

Nova Fitness Co. Ltd: Laser $PM_{2.5}$ Sensor specification, SDS011. Version V1.3. Data sheet, https://cdn-reichelt.de/documents/datenblatt/X200/SDS011-DATASHEET.pdf, 2015

Popoola, O. A. M., Stewart, G. B., Mead, M. I. and Jones, R. L.: Development of a baseline-temperature correction methodology for electrochemical sensors and its implications for long-term stability. Atmos. Environ., 147, 330–343, https://doi.org/10.1016/j.atmosenv.2016.10.024, 2016

Rao, S. T., Samson, P. J. and Peddada, A. R.: Spectral analysis approach to the dynamics of air pollutants. Atmos. Environ., 10, 375–379, 10.1016/0004-6981(76)90005-6, 1976

Sebald, L., Treffeisen, R., Reimer, E. and Hies, T.: Spectral analysis of air pollutants. Part 2: ozone time series. Atmos. Environ., 34, 3503–3509, https://doi.org/10.1016/S1352-2310(00)00147-3, 2000

Seinfeld, J. H. and Pandis, S. N.: Atmospheric Chemistry and Physics, third edition, John Wiley and Sons, Hoboken New Jersey, 2016

585 SGX Sensortech: The MiCS-6814 is a compact MOS sensor with three fully independent sensing elements on one package. 1143 rev 8. Data Sheet, https://www.sgxsensortech.com/content/uploads/2015/02/1143_Datasheet-MiCS-6814-rev-8.pdf, 2015

Snyder, E. G., Watkins, T. H., Solomon, P. A., Thoma, E. D., Williams, R. W., Hagler, G. S. W., Shelow, D., Hindin, D. A., Kilaru, V. J. and Preuss, P. W.: The changing paradigm of air pollution monitoring. Environ. Sci. Technol., 47, 11369-11377, https://doi.org/10.1021/es4022602, 2013

590 Spinelle, L., Gerboles, M., Villani, M. G., Aleixandre, M. and Bonavitacola, F.: Field calibration of a cluster of low-cost available sensors for air quality monitoring. Part A: Ozone and nitrogen dioxide. Sens. Actuators B Chem, 215, 249-257, https://doi.org/10.1016/j.snb.2015.03.031, 2015

Spinelle, L., Gerboles, M., Villani, M. G., Aleixandre, M. and Bonavitacola, F.: Field calibration of a cluster of low-cost commercially available sensors for air quality monitoring. Part B: NO, CO and CO_2. Sens. Actuators B Chem, 238, 706-715,
595 https://doi.org/10.1016/j.snb.2016.07.036, 2017

Stetter, J.R. and Li, J.: Amperometric gas sensors: A review, Chem. Rev., 352—366, 108, https://doi.org/10.1021/cr0681039, 2008

Stohl, A., Eckhardt, S., Forster, C., James, P. and Spichtinger, N.: On the pathways and timescales of intercontinental air pollution transport, J. Geophys. Res. Atmos., ACH 6-1-ACH 6-17, 107, D23, https://doi.org/10.1029/2001JD001396, 2002

Sun, G., Hazlewood, G., Bernatsky, S., Kaplan, G. G., Eksteen, B. and Barnabe, C.: Association between air pollution and the development
600 of rheumatic disease: a systematic review. Int. J. Rheumatol., https://doi.org/10.1155/2016/5356307, 2016

Sun, L. and Wang, M.:Global warming and global dioxide emission: An empirical study. J. Environ. Manage., 46, 327-343, https://doi.org/10.1006/jema.1996.0025, 1996

Sun, L. and Wang, M.: A component time-series model for SO_2 data: Forecasting, interpretation and modification. Atmos. Environ., 31, 9, 1285-1295, https://doi.org/10.1016/S1352-2310(96)00306-8, 1997

605 Sun, L. and Westerdahl, D. and Ning, Z.: Development and evaluation of a novel and cost-effective approach for low-cost NO_2 sensor drift correction. Sensors, 17, 8, 1916, https://doi.org/10.3390/s17081916, 2017

Tchepel, O., Costa, A. M., Martins, H., Ferreira, J., Monteiro, A., Miranda, A. I. and Borrego, C.: Determination of Background Concentrations for Air Quality Models Using Spectral Analysis of Monitoring Data. Atmos. Environ., 44, 1, 106-114, https://doi.org/10.1016/j.atmosenv.2009.08.038, 2009

610 Uria-Tellaetxe, I. and Carslaw, D. C.: Conditional bivariate probability function for source identification. Environ. Model. Softw., 59, 1-9, https://doi.org/10.1016/j.envsoft.2014.05.002, 2014

Van de Hulst, H.C.: Light scattering by small particles, Dover Publications, Inc., New York, 1981

Van der Hoven, I.: Power spectrum of horizontal wind speed in the frequency range from 0.0007 to 900 cycles per hour. J. Meteorology, 14, 160–164, https://doi.org/10.1175/1520-0469(1957)014<0160:PSOHWS>2.0.CO;2, 1957

615 Venter, Z. S., Aunan, K., Chowdhury, S. and Lelieveld, J.: COVID-19 lockdowns cause global air pollution declines. PNAS, 117, 32, 18984-18990, https://doi.org/10.1073/pnas.2006853117, 2020

Vignati, E., Berkowicz, R., and Hertel, O.: Comparison of air quality in streets of Copenhagen and Milan, in view of the climatological conditions. Sci. Total Environ., 189/190, 467-473, http://dx.doi.org/10.1016/0048-9697(96)05247-3, 1996

Viricelle, J. P. and Pauly, A. and Mazet, L. and Brunet, J. and Bouvet, M. and Varenne, C. and Pijolat, C.: Selectivity improve-
620 ment of semi-conducting gas sensors by selective filter for atmospheric pollutants detection. Mater. Sci. Eng. C., 26, 2-3, 186–195, https://doi.org/10.1016/j.msec.2005.10.062, 2006

Wang, W., Liu, C., Ying, Z., Lei, X., Wang, C., Huo, J., Zhao, Q., Zhang, Y., Duan, Y., Chen, R. and Fu, Q.: Particulate air pollution and ischemic stroke hospitalization: How the associations vary by constituents in Shanghai, China. Sci. Total Environ., 695, 133780, https://doi.org/10.1016/j.scitotenv.2019.133780, 2019

625   Wang, Z., Zhong, S., Peng, Z.R. and Cai, M.: Fine-scale variations in $PM_{2.5}$ and black carbon concentrations and corresponding influential factors at an urban road intersection. Build. Environ., 141, 215-225, https://doi.org/10.1016/j.buildenv.2018.04.042, 2018

Westmoreland, E. J and Carslaw, N. and Carslaw, D. C. and Gillah, A. and Bates, E.: Analysis of air quality within a street canyon using statistical and dispersion modelling techniques. Atmos. Environ., 41, 39, 9195–9205, https://doi.org/10.1016/j.atmosenv.2007.07.057, 2007

630   WHO. Ambient (outdoor) air pollution. Technical Report Version V1, World Health Organization, 2021.

Wilson, J. G., Kingham, S., Pearce, J. and Sturman, A. P.: A review of intraurban variations in particulate air pollution: Implications for epidemiological research. Atmos. Environ., 39, 34, 6444-6462, https://doi.org/10.1016/j.atmosenv.2005.07.030, 2005

Wu, Z., Zhang, Y., Zhang, L., Huang, M., Zhong, L., Chen, D. and Wang, X.: Trends of outdoor air pollution and the impact on premature mortality in the Pearl River Delta region of southern China during 2006–2015. Sci. Total Environ., 690, 248-260,
635   https://doi.org/10.1016/j.scitotenv.2019.134390, 2019

Zhang, H., Dong, H., Ren, M., Liang, Q., Shen, X., Wang, Q., Yu, L., Lin, H., Luo, Q., Chen, W. and Knibbs, L.D.: Ambient air pollution exposure and gestational diabetes mellitus in Guangzhou, China: A prospective cohort study. Sci. Total Environ., 699, 134390, https://doi.org/10.1016/j.scitotenv.2019.134390, 2020

Zou, B., Wilson, J. G., Zhan, F. B. and Zeng, Y.: Spatially differentiated and source-specific population exposure to ambient urban air
640   pollution. Atmos. Environ., 43, 26, 3981-3988, https://doi.org/10.1016/j.atmosenv.2009.05.022, 2009